Nuclear Instruments and Methods in Physics Research Section B: Beam Interactions with Materials and Atoms 354 (2015): 9-15
DOI: https://doi.org/10.1016/j.nimb.2014.11.009

Scattering of H(D) from LiF(100) under fast grazing incidence conditions: To what extent is classical dynamics a useful tool?

A. S. Muzas[a], F. Martín[a,b], C. Díaz[a,*]

[a] *Departamento de Química Módulo 13, Universidad Autónoma de Madrid, 28049 Madrid, Spain*
[b] *Instituto Madrileño de Estudios Avanzados en Nanociencias (IMDEA-nanociencia), Cantoblanco 28049 Madrid, Spain*

Abstract

Diffraction experiments of atoms and molecules under fast grazing incidence conditions have opened a new field in surface science. This experimental effort calls for complementary theoretical studies, which would allow a detailed analysis of experimental data. Here, we have analyzed the ability of classical dynamics simulations to reproduce experimental results. To perform this study, a DFT (Density Functional Theory) based potential energy surface, describing the interaction between a H atom and a LiF(100) surface, has been computed. Diffraction probabilities have been simulated by means of a classical binning method. Our results have been found to be in qualitative good agreement with recent experimental measurements.

Keywords: Grazing incidence, scattering, classical dynamics

PACS: 34.35.+a, 68.49+Df, 82.65.+r

*Corresponding author
Email address: cristina.diaz@uam.es (C. Díaz)

1. Introduction

Since its theoretical prediction [1, 2], and especially, since the first independent experimental measurements few years later [7, 8], the diffraction of atoms and molecules from surfaces under fast grazing incidence (FGI) conditions has attracted much attention (see Ref. [10] and references therein), mainly due to its potential use as a surface analysis tool.

As already discussed in the literature [2, 8, 11, 12], the physical mechanism behind this phenomenon is the strong decoupling between the fast motion parallel to the surface, and the slow motion normal to it. Due to the grazing incidence conditions, the potential felt by the projectile is periodic (or quasi-periodic). If we apply the perturbation theory to the case of a classical particle moving on a periodic potential [13], it can be seen that the parallel momentum change along the incidence direction x is given by $\Delta K_x = -\frac{1}{v_x}\int_0^a dx \frac{\partial V(x,y)}{\partial x} = 0$, a being the parameter periodicity of the potential along the incidence direction, V the potential felt by the projectile, and v_x its velocity. In contrast, the parallel momentum change along the perpendicular direction, y, is given by $\Delta K_y = -\frac{1}{v_x}\int_0^a dx \frac{\partial V(x,y)}{\partial y} \neq 0$. Therefore, the change of the wave vector along this direction is zero (or almost zero). Thus, any significant change of the parallel wave vector ($\mathbf{K}$), induced in the projectile when approaching the surface, is due to a transfer of momentum from the slow motion, normal to the surface, to the motion parallel to the surface, and perpendicular to the incidence direction. At this point, it should be remembered that diffraction occurs whenever the change of the parallel wave vector ($\mathbf{K}_f$-$\mathbf{K}_i$) coincides with a reciprocal lattice vector ($\mathbf{G}_{n,m}$), $\mathbf{K}_i$ and $\mathbf{K}_f$ being the initial and final parallel wave vector, respectively. And that the de

Broglie wave length associated with the slow normal motion ($\lambda = 2\pi/k_\perp$) is of the order of magnitude of $\mathbf{G}_{n,m}$, which allows the observation of diffraction.

Diffraction under FGI conditions has been already observed for many different systems, including atomic (Ar, Ne, He and H) and molecular (H_2) projectiles, and a wide variety of surfaces [10]. First measurements were performed in 2007 on insulators, LiF(100) [7, 8] and NaCl(001) [8, 14]. At that time, it was unclear whether diffraction from metal surfaces could be measured, due to electronic excitations. But one year later, first diffraction measurements from a metal surface were published [15]. Since then, grazing incidence experiments have been performed in a wide diversity of systems: He, Ne, Ar, N/KCl(001) [16]; He/Ni(110) [17]; He, Ar/Al(111)[18]; He, H_2/Mo(112) [19]; He/Ag(110) [20]; He/monolayer of silica in Mo(112) [21]; He/c(2 $\times$ 2) reconstructed ZnSe(001) [22]; He, H_2/c(2×2)S-Fe(110) and he, H_2/c(1×3)O-Fe(110) [23]; He/c(2×4)O-Mo(112) [24]; H/$Al_2O_3(11\bar{2}0)$ [25]; H, He/MgO(001) [26]. However, diffraction of H and, in particular, He atoms from LiF(100) is still the most studied system [27, 28, 29, 30, 31, 32]. Among theses experimental studies, it is worth mentioning the study of decoherence induced by electronic excitations carried out by Winter et al.[31, 32] for H and He/LiF(100). They have shown, on the one hand, that electronic excitations are far more important for H than for He atoms, in contrast to previous studies for slow projectiles scattered from metal surfaces [33]. And, on the other hand, they have shown that, even in the case of H atoms, the decoherece induced by the electronic excitations in the scattering process is not strong enough to prevent diffraction.

This experimental effort has inspired a number of theoretical studies.

For example, Ruiz et al. [34, 35] have studied the momentum and the energy transfer between the intramolecular degrees of freedom (DOF's) in the quasiresonance region, using classical trajectory calculations and a diatom-rigid surface collision model. Classical trajectory calculations have also been used to study classical rainbow angles [16]. In this latter study, Hartree-Fock based pair potentials were employed. But, subsequent semiclassical studies, using DFT (density functional theory) based potentials, have shown that superposition of interatomic pair potentials may not be adequate to describe atom/surface interactions under FGI conditions [19, 18]. Schüller et al. [26], using a semiclassical approach, have shown that potentials based on superposition of individual Hartree-Fock pair potentials describe fairly well classical scattering phenomena, whereas DFT based potentials are needed to describe diffraction for normal incidence energies below 0.1 eV. Angular distributions and interference structures have been investigated by means of the surface eikonal approximation [36, 29], and very recently [37, 20] by using a three-dimensional (3D) potential energy surface (PES), obtained by applying the corrugation reducing procedure (CRP) method to a set of DFT data points. Mason et al. [38] have developed a theory based on quantum-mechanical transition rates, aiming to study thermal effects. These thermal effects have also been studied using a quantum trajectory Monte Carlo method [28, 30].

Here, we have analyzed to what extent classical dynamics can be used to analyze experimental measurements of scattering (and diffraction) of atoms from surface under FGI conditions. The reliability of our study is supported by previous studies, performed for molecular diffraction at thermal and quasi-thermal energies [3, 4, 5, 6, 48, 50], showing that a classical binning method,

proposed for the first time by Bowman et al. [3, 4], is able to reproduce qualitatively quantum theoretical and experimental diffraction peaks. The binning method should work better under FGI conditions, because the parallel momentum change (respect to the total momentum) leading to diffraction is smaller than in the case of thermal energies.

2. Theoretical approach

Taking advantage of the different time scales of the nuclear and electronic motions, we describe the interaction between the atoms and the surface within the Born-Oppenheimer approximation (BOA). The validity of the BOA is supported by recent experiments [31] showing that, although there are electronic excitations inducing decoherence in the system, they neither suppress completely nor modify the diffraction patterns. In fact, in Ref. [31] it was shown that diffraction can be observed experimentally for total energies (E_T) up to 1 keV and incidence angles (θ_i) up to 1.7 deg. -see Fig. 1 (b) for the definition of the diffraction angles. In Ref. [31], it was also shown that diffraction patterns could be recorded for higher E_T values (up to ≈ 1.5 keV) using smaller θ_i values.

The 3D PES, describing the electronic structure of the system, has been computed by applying the CRP method of Busnengo et al. [39] to a set of DFT-GGA (density functional theory within the generalized gradient approximation) data. Within the CRP scheme, the 3D PES (V_{3D}) is written as:

$$V_{3D}(\mathbf{R}) = I_{3D}(\mathbf{R}) + \sum_{i=1}^{n} V_{1D}^{Li}(\mathbf{r}_i) + \sum_{i=1}^{n} V_{1D}^{F}(\mathbf{r}_i), \quad (1)$$

where $\mathbf{R}$ represents the Cartesian coordinates of the H atom over the surface

and $\mathbf{r}_i$ the distance between the H atom and the Li or F atom. The smooth I_{3D} function has been interpolated over Z using third-order cubic splines, and over (X, Y) using a symmetry adapted Fourier expansion. The DFT-GGA data set contains 510 single points energy values, computed over the six sites shown in Fig. 1 (a). For each site, 85 DFT single point energies for Z values between -1.16 $\mathring{A}$ and 5.45 $\mathring{A}$ have been evaluated. The overall errors in the fitting procedure are found to be smaller than 1%. DFT calculations have been performed with the package VASP [40, 40, 41]. In applying the GGA, the PW91 functional [42] has been used. The PAW (projector augmented wave) method [43] is used to describe the ion cores. And to model the system adsorbate/substrate a five-layer slab and a (2×2) surface unit cell have been used. To avoid artifacts caused by the use of periodic boundary conditions in the direction perpendicular to the slab, a vacuum layer of 20 $\mathring{A}$ has been placed between the slabs in the z direction. The plane-wave expansion has been limited by a cutoff energy of 800 eV, and a $5 \times 5 \times 1$ k-point grid has been used to sample the Brillouin zone. Using these parameters, the lattice constant (see Fig 1) has been found to be 2.88 $\mathring{A}$, in good agreement with previous theoretical results [30, 44] and with the experimental value of 2.84 $\mathring{A}$ [45]. The interlayer distance after relaxation has been found to be 1.98 $\mathring{A}$, the top-most layer presents a rumpling of 0.065 $\mathring{A}$, with the F^- ions displaced outwards and the Li^+ ions inwards, in good agreement with previous theoretical calculations [46, 47, 30].

In Fig. 2 we display several 2D(x,y) cuts showing the characteristics of the interpolated 3D-PES. From this plot it can be seen that far from the surface (Z $\geq$ 1.66 $\mathring{A}$) the potential over the F (V_{1D}^F) ion is higher than over the Li

(V_{1D}^{Li}) ion. For distances around Z=1.5 $\mathring{A}$, both potentials are very similar. Closer to the surface (1.33 $\mathring{A} \leq$ Z), $V_{1D}^{Li} > V_{1D}^{F}$. When the H atom reaches shorter distances Z ≤ 0.6 $\mathring{A}$ (do no show in Fig. 2) V_{1D}^{F} becomes higher than V_{1D}^{Li} once again. The corrugation complexity of this PES is reflected in the diffraction patterns, as we discussed in Sec. 3.

To study the scattering of H atoms from LiF(100), we have performed classical calculations [48, 11]. Within the classical dynamics framework, a classical trajectory is computed by solving the Hamilton equations of motion. The classical scattering probability as a function of the polar angle, θ_i, (see Fig. 1 (b)), and the incidence energy (E_T) is calculated as an average over 15000 trajectories, which ensures low statistical errors. But, in order to compare our theoretical simulations with experimental measurements, diffraction probabilities have to be evaluated. Since diffraction is a quantum phenomenon related to discrete changes of the parallel wave vector, in principle, quantum calculations would be needed. However, as already shown in the case of diffraction of molecules at low incidence energy [3, 4, 49], molecular and atomic diffraction can be qualitatively evaluated by means of a classical binning method. In this case, the intensity of a given diffraction peak (n, m) is evaluated as the fraction of classical trajectories in which the atoms scatter with a parallel momentum change ($\Delta P_{||}=\hbar K$) contained in the 2D Wigner-Seitz cell of the (n, m) lattice point in reciprocal space (see Fig. 3). In particular, this method has shown to be able to mimic fairly well the relative intensities of the experimental diffraction spectra of H_2/Pd(111) [48], H_2/Cu(111) and H_2/Cu/Ru(0001) [50].

3. Results and discussion

In order to test the classical binning method, a detailed comparison between experimental and theoretical simulated diffraction spectra have been performed. In Fig. 4 (b) we show the diffraction pattern of H/LiF(100) for E_T=0.8 keV and θ_i=1.48 deg. obtained by Winter et al. [10]. This spectrum shows, additionally to the specular peak, first and second order peaks. Furthermore, the first order peaks are more intense than the specular one. Our classical theoretical simulations, displayed in Fig. 4 (a), show the same trend, i.e., five peaks are present in the spectrum, and the first order peaks are more intense that the specular one, which supports the suitability of our method. At this point, it is should be noticed that in order to compare with this experimental spectrum, our delta-shape theoretical diffraction probabilities have been convoluted using a Gaussian function.

The above comparison is merely qualitative, a more quantitative comparison is shown in Fig. 5. In this figure we compare our classical results with the diffractogram obtained by Rousseau et al. [9] for diffraction of H atoms along the $< 100 >$ direction. This experimental spectrum shows that the first order peaks are more intense that the specular one, for a normal energy E_z=300 meV. From this figure we observe that our theoretical calculations reproduce the experimental results with a shift of 100 meV. As it could be expected, classical diffraction probabilities can not reproduce quantitatively the experimental probabilities, but they are able to reproduce the experimental trend. This would be more clearly seen if a set of experimental results for different normal energies were available.

Although, to our knowledge, experimental data as a function of the nor-

mal energy have not been systematically recorded for H/LiF(100), we show this study in Fig. 6. In this figure we have displayed a series of theoretical diffractograms as a function of the normal energy, for a total energy (incidence angle) between 1.0 keV (0.81 deg.) and 2.0 keV (1.21 deg.), for diffraction along the crystallographic directions $< 110 >$ and $< 100 >$. At this point, it should be pointed out that, to avoid spurious results on the simulated diffraction probabilities due to the classical rainbow effect, [51], classical trajectories with a final azimuthal angle $\phi \geq \phi_{CR}^{+} - 0.005i\ deg.$ or $\phi \leq \phi_{CR}^{-} + 0.005\ deg.$ are not taken into account during the binning procedure. In these two equations ϕ_{CR}^{+} and ϕ_{CR}^{-} represent the positive and negative rainbow angle, repectively (see 6 and 7).

From Fig. 6 several interesting properties of this system are observed: (i) The normal energy for which the first order peaks become higher than the specular peak is smaller for incidence along the $< 100 >$ direction, in good agreement with experimental results by Rousseau and et al. [9]. These authors have shown that along the $< 110 >$ direction, the specular peak is still more intense than the first order ones for E_z=560 meV; (ii) The number of diffraction peaks, along the $< 100 >$ direction is higher than along the $< 110 >$ direction, despite the fact that the parallel momentum change required to excite a diffraction peak along the $< 110 >$ direction is smaller than the one required to excite a peak along the $< 100 >$ one. This latter result also agrees with the experimental findings [9]. Thus, both experiment and theory agree in the fact that the corrugation felt by the atoms is higher along the $< 100 >$. It is also worthy to mention that the experimental diffraction spectra recorded for H_2 and He show, as expected, more diffraction

along the $< 110 >$. The unexpected results obtained for H/LiF(100) reveal the complexity of the system, which is essentially captured by the classical binning method.

The complexity of H/LiF(100) may be understood by turning our attention to the geometrical structure factor, because the amplitude of the diffraction peaks, for polyatomic surfaces, depends on it. The geometrical structure factor can be written as a function of the atomic form factors as:

$$S_G = f_{Li}(\mathbf{G})e^{i\mathbf{G}\mathbf{d}_{Li}} + f_F(\mathbf{G})e^{i\mathbf{G}\mathbf{d}_F} \tag{2}$$

where f_{Li} and f_F are the atomic form factors for Li and F ions, respectively. $\mathbf{G} = n\mathbf{b}_1 + m\mathbf{b}_2$ represents the reciprocal lattice for LiF(100), and $\mathbf{d}_{Li}$ and $\mathbf{d}_F$ are the atomic basis set vectors. From Eq. 2 we see that S_G is equal to $f_{Li} + f_F$ if $n+m$ is an even number, and equal to $f_{Li} - f_F$ if $n+m$ is an odd number. This equation reveals the first remarkable difference between the two incidence directions. All the diffraction peaks observed along the $< 100 >$ direction correspond to $n + m$=even, i.e., for all them $S_G = f_{Li} + f_F$. On the other hand, diffraction along the $< 110 >$ direction shows peaks with $n+m$ even and odd alternately, which may explain the stronger modulation on this direction. It should be also remembered that the atomic form factors depend on the electronic density, i.e., there is a close relationship between the form factors and the corrugation of the PES, which varies quite a lot as a function of the distance to the surface (see Fig. 3). Thus, depending on the classical turning point (z_{av}), $f_{Li} + f_F$ could be similar to $f_{Li} - f_F$, if $f_{Li} >> f_F$ or $f_{Li} << f_F$, or very different, if $f_{Li} \approx f_F$. This phenomenon could explain the results displayed in Fig. 6. At this point, it should be noticed that this explanation holds independently of the projectile. And, that the

different behavior observed for different proyectiles depends on the specific values of the form factors, and therefore, on the corrugation of PES for each projectile/surface system.

For the sake of completeness, in Figs. 6 and 7 we have also included the raw classical reflection probabilities, which show the classical rainbow peaks. Interestingly, the angular distributions obtained for the $< 110 >$ direction show four rainbow peaks, whereas, for the $< 100 >$ direction, they only show two. This is a consequence of the average periodic potential: while in the former case, the potential exhibits two different maxima, over the F-F and Li-Li rows (see Fig. 2-4, Ref [10]), in the latter case, it only exhibits one maximum, over the F-Li rows, and one minimum. Furthermore, in the case of the $< 110 >$ direction, only two rainbow peaks are observed for the incidence conditions, $E_T = 1.3$ keV, $\theta_i = 1.07$ $deg.$ (see Figs. 6 and 7), for which the classical turning point (z_{av}) is located in a region where the potential over the F atoms is similar to the potential over the Li atoms (see Fig. 2).

Finally, we have also corroborated that changing H by D atoms in our classical simulations leads to entirely different diffraction patterns (see Fig. 7). At the same energy, a D atom is slower than a H atom, and therefore, its de Broglie wavelength is smaller, which implies that, for the same energy, the diffraction spectra measured for deuterium present a different peaks distribution than the ones measured for hydrogen. This behavior is observed in our classical simulations (see Figs. 6 and 7). Unfortunatelly, to our knowledge, D/LiF(100) experimental diffractograms are not available in the literature. Those experimental measurements would help us to futher assay our classical

binning method.

4. Summary

In this manuscript we have analyzed to what extent classical dynamics can be used to analyze experimental results on scattering of atoms under FGI conditions. To perform this study we have used an accurate potential energy surface (PES) built by interpolation of a DFT data set. We have shown that diffraction probabilities obtained using a classical binning method reproduce fairly well the experimental trends. Thus, classical dynamics can be used to perform coarse analysis, which could be used to lead the quantum dynamics simulations to the systems and incidence conditions of most interest. These coarse analyses will be even more useful for molecules/surface systems, for which quantum dynamics simulations are very time-consuming from a computational point of view.

Acknowledgements

We are very grateful to H. F. Busnengo for useful discussions about the CRP method. We thank CCC-UAM for allocation of computer time. Work supported by MICINN project FIS2010-15127.

References

[1] E. A. Andreev, Russ. J. Phys. Chem. 76 (2002) 164.

[2] D. Farías, C. Díaz, P. Nieto, A. Salin, F. Martín, Chem. Phys. Lett. 390 (2004) 250.

[3] J. Ray, J. M. Bowman, J. Chem. Phys. 63 (1975) 5231.

[4] J. Ray, J. M. Bowman, J. Chem. Phys. 66 (1977) 1122.

[5] S. C. Park, J. M. Bowman, Chem. Phys. Lett. 110 (1984) 383.

[6] S. Saini, D. A. Dows, H. S. Taylor, Chem. Phys. 90 (1984) 87.

[7] A. Schüller, S. Wethekam, H. Winter, Phys. Rev. Lett. 98 (2007) 016103–1.

[8] P. Rousseau, H. Khemliche, A. G. Borisov, P. Roncin, Phys. Rev. Lett. 98 (2007) 016104–1.

[9] P. Rousseau, H. Khemliche, N. Bundaleski, P. Soulisse, A. Momeni, P. Roncin, J. Phys.: Confer. Series 133 (2008) 012013.

[10] H. Winter, A. Schüller, Prog. Surf. Sci 86 (2011) 169.

[11] C. Díaz, P. Rivière, F. Martín, Phys. Rev. Lett. 103 (2009) 013201.

[12] C. Díaz, F. Martín, Phys. Rev. A 82 (2010) 012901.

[13] A. Salin, Eur. Phys. J. D 8 (2000) 189.

[14] B. Lalmin, H. Khemliche, A. Momeni, P. Soulisse, P. Roncin, J. Phys.: Condes. Matter 24 (2012) 442002.

[15] N. Bundaleski, H. Khemliche, P. Soulisse, P. Roncin, Phys. Rev. Lett. 101 (2008) 177601.

[16] U. Specht, M. Busch, J. Seifert, H. Winter, K. Gärtner, R. Wlodarczyk, M. Sierka, J. Sauer, Nucl. Instrum. Methods Phys. Res. B 269 (2011) 799.

[17] M. Busch, A. Schüller, S. Wethekam, H. Winter, Surf. Sci. 603 (2009) L23.

[18] P. Tiwald, A. Schüller, H. Winter, K. Tökesi, F. Aigner, S. Gräfe, C. Lemell, J. Burgdörfer, Phys. Rev. B 82 (2010) 125453.

[19] J. Seifert, A. Schüller, H. Winter, R. Wlodarczyk, J. Sauer, M. Sierka, Phys. Rev. B 82 (2010) 035436.

[20] C. A. Ríos-Rubiano, G. A. Bocan, M. S. Gravielle, N. Bundaleski, H. Khemliche, P. Rocin, Phys. Rev. A 87 (2013) 012903.

[21] J. Seifert, H. Winter, Surf. Sci. 603 (2009) L109.

[22] H. Khemliche, P. Rousseau, P. Roncin, V. H. Etgens, F. Finocchi, Appl. Phys. lett. 95 (2009) 151901.

[23] A. Schüller, M. Busch, J. Seifert, S. Wethekam, H. Winter, Phys. Rev. B 79 (2009) 235425.

[24] J. Seifert, H. Winter, Phys. Rev. Lett. 108 (2012) 065503.

[25] M. Busch, J. Seifert, E. Meyer, H. Winter, Phys. Rev. B 86 (2012) 241402.

[26] A. Schüller, D. Blauth, J. Seifert, M. Busch, H. Winter, K. Gärtner, R. Wlodarczyk, J. Sauer, M. Sierka, Surf. Sci. 606 (2012) 161.

[27] A. Schüller, H. Winter, Phys. Rev. Lett. 100 (2008) 097602–1.

[28] F. Aigner, N. Simonović, B. Solleder, L. Wirtz, J. Burgdörfer, Phys. Rev. Lett. 101 (2008) 253201.

[29] A. Schüller, H. Winter, M. S. Gravielle, J. M. Pruneda, J. E. Miraglia, Phys. Rev. A 80 (2009) 062903.

[30] A. Schüller, S. Wethekam, D. Blauth, H. Winter, F. Aigner, N. Simonović, B. Solleder, J. Burgdörfer, L. Wirtz, Phys. Rev. A 82 (2010) 062902.

[31] J. Lienemann, A. Schüller, D. Blauth, J. Siefert, S. Wethekam, M. Busch, K. Maass, H. Winter, Phys. Rev. Lett. 106 (2011) 067602–1.

[32] M. Busch, J. Lienemann, J. Seifert, A. Schüller, H. Winter, Vacuum 86 (2012) 1618.

[33] H. Winter, J. I. Juaristi, I. Nagy, A. Arnau, P. M. Echenique, Phys. Rev. B 67 (2003) 245401.

[34] A. Ruiz, J. P. Palao, E. J. Heller, Phys. Rev. A 79 (2009) 052901.

[35] A. Ruiz, J. P. Palao, J. Chem. Phys. 137 (2012) 084302.

[36] M. S. Gravielle, J. E. Miraglia, Phys. Rev. A 78 (2008) 022901.

[37] M. S. Gravielle, G. A. Bocan, R. Díez-Muiño, Phys. Rev. A 82 (2010) 052904.

[38] J. R. Manson, H. Khemliche, P. Roncin, Phys. Rev. B 78 (2008) 155408.

[39] H. F. Busnengo, A. Salin, W. Dong, J. Chem. Phys. 112 (2000) 7641.

[40] G. Kresse, J. Hafner, Phys. Rev. B 47 (1993) 558.

[41] G. Kresse, J. Furthmüller, Phys. Rev. B 54 (1996) 11169.

[42] J. P. Perdew, J. A. Chevary, S. H. Vosko, K. A. Jackson, M. R. Pederson, D. J. Singh, C. Fiolhais, Phys. Rev. B 46 (1992) 6671.

[43] P. E. Blöchl, Phys. Rev. B 50 (1994) 17953.

[44] N. A. Smirnov, Phys. Rev. B 83 (2011) 014109.

[45] J. Liu, L. Dubrovinsky, T. Boffa-Ballaran, W. Crichton, High Pressure Res. 27 (2007) 483.

[46] F. W. de Wette, W. Kress, U. Schröder, Phys. Rev. B 32 (1985) 4143.

[47] N. P. Wang, M. Rohlfing, P. Krüger, J. Pollmann, Phys. Rev. B 67 (2003) 115111.

[48] D. Farías, C. Díaz, Rivière, H. F. Busnengo, P. Nieto, M. F. Somers, G. J. Kroes, A. Salin, F. Martín, Phys. Rev. Lett. 93 (2004) 246104.

[49] C. Díaz, H. F. Busnengo, P. Rivière, D. Farías, P. Nieto, M. F. Somers, G. J. Kroes, A. Salin, F. Martín, J. Chem. Phys. 122 (2005) 154706.

[50] C. Díaz, F. Martín, G. J. Kroes, M. Minniti, D. Farías, R. Miranda, J. Phys. Chem. C 116 (2012) 13671.

[51] S. Miret-Artés, E. Pollak, Surf. Sci. Rep. 67 (2012) 161.

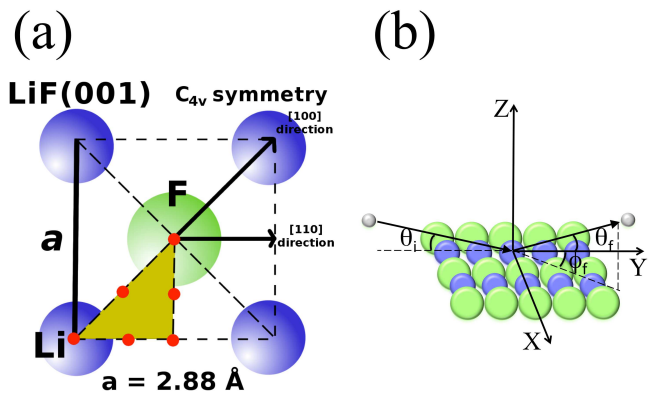

Figure 1: (a) Schematic representation of the LiF(100) unit cell. Red dots represent the configurations used to computed the DFT data set. (b) Schematic representation of a grazing incidence collision of H with a LiF(100) surface. The coordinate system used in the dynamics is also shown.

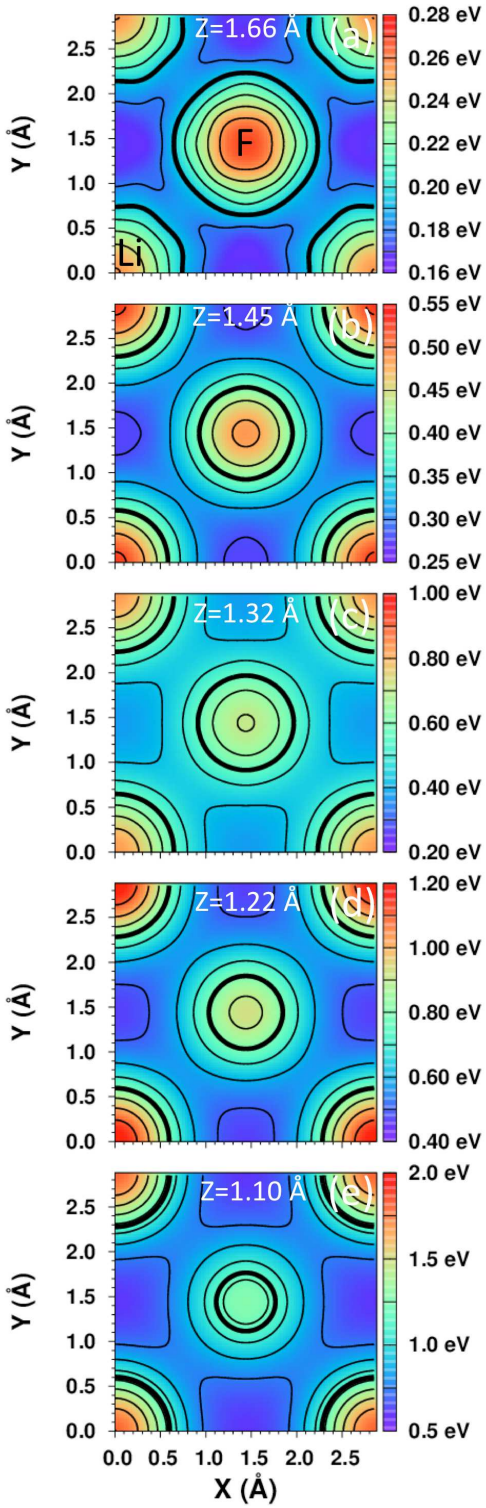

Figure 2: 2D (X,Y) cuts. (a) Z=1.66 $\AA$ with a contour level spacing ΔE=0.015 eV, the thick black line (TBL) represents an energy value of 0.195 eV; (b) Z=1.45 $\AA$ with ΔE=0.04 eV and TBL=0.40 eV; (c) Z=1.32 $\AA$ with ΔE=0.07 eV and TBL=0.56 eV; (d) Z=1.22 $\AA$ with ΔE=0.1 eV and TBL=0.8 eV; (e) Z=1.10 $\AA$ with ΔE=0.15 eV and TBL=1.15 eV.

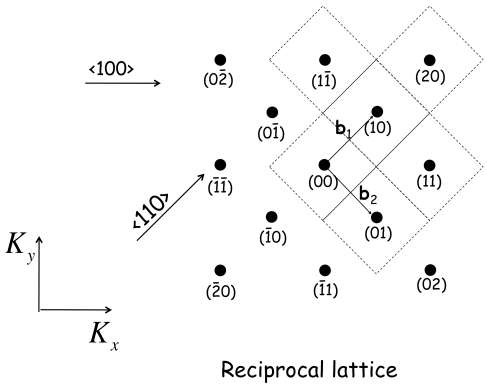

Figure 3: Reciprocal lattice of LiF(100). The dotted lines demarcate the 2D Wigner-Seitz cells around each lattice point. Number within parentheses indicate the corresponding Miller indices. Numbers within brackets indicate the incidence direction considered in this work.

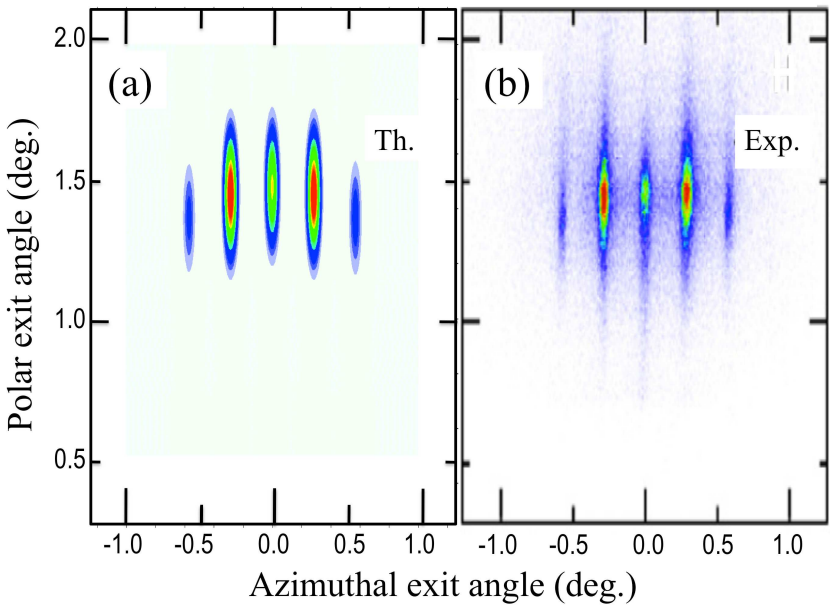

Figure 4: (a) 2D (θ_f,ψ_f) calculated intensities for the diffraction spectrum along the incidence direction $<$ 100 $>$ for E_T=0.8 keV and θ_i=1.48 deg. 2D results have been convoluted with a 2D Gaussian function of width σ_ϕ=0.025 deg. and σ_θ=0.12 deg. to simulate a typical experimental resolution. (b) Diffraction spectrum measured by Winter et al. taking from Ref. [10].

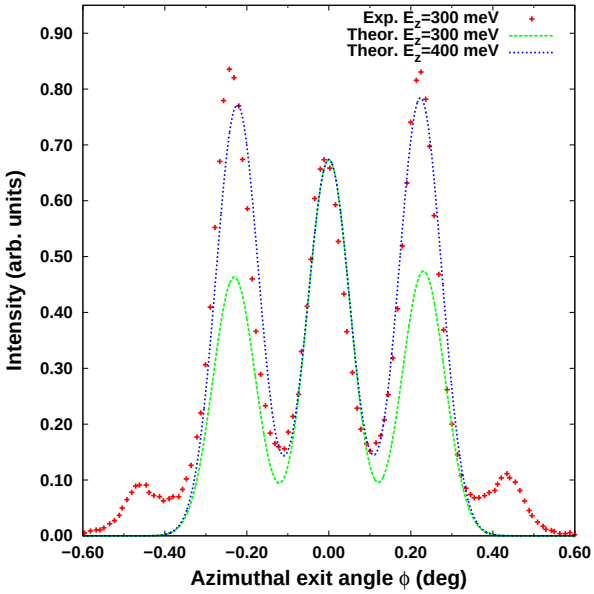

Figure 5: Diffraction spectrum of H/LiF(001) along the $< 100 >$ direction. Red crosses: Experimental data from Ref. [9]. Dashed and dotted lines: Classical theoretical results, which have been convoluted with a 1D Gaussian function of width σ_ϕ=0.052 deg. to simulate the experimental resolution. E_z is the normal energy.

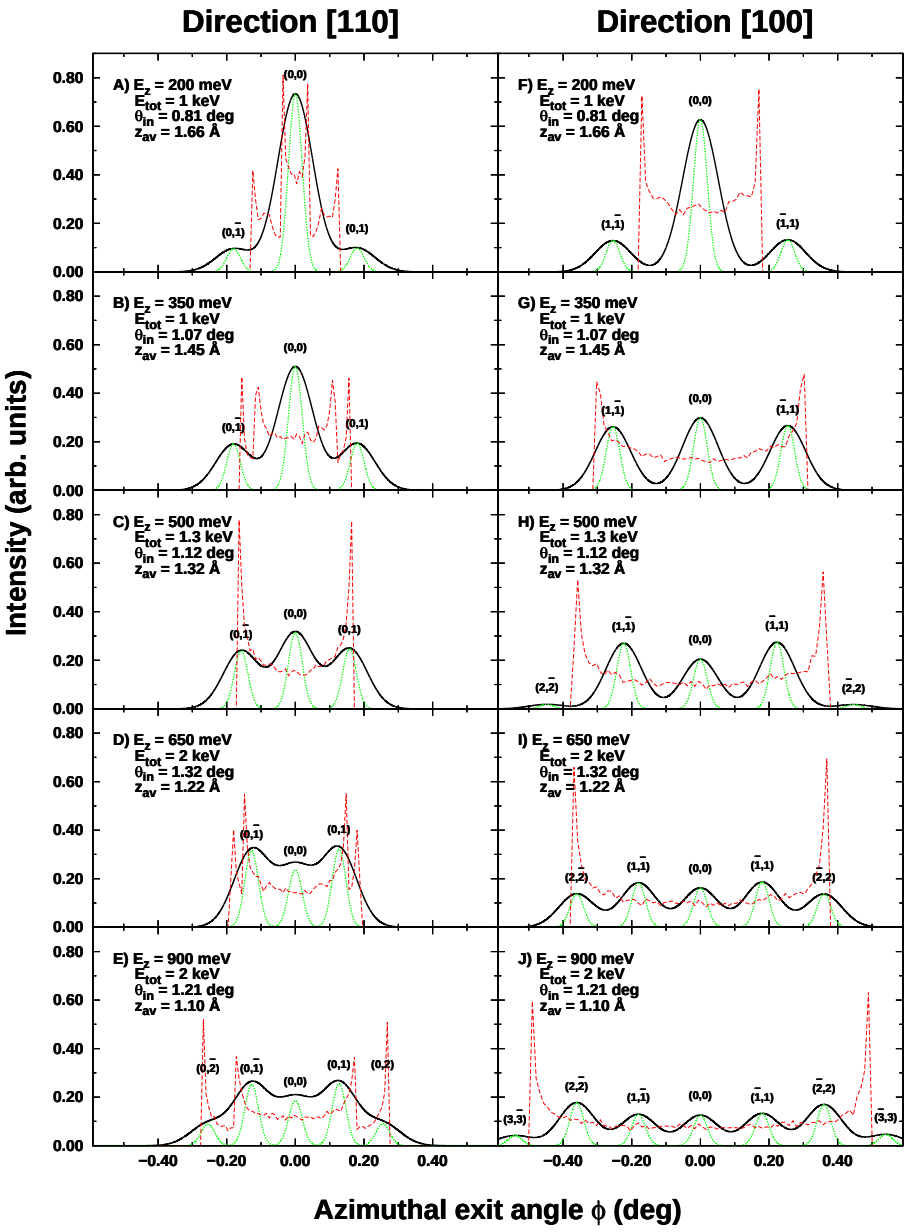

Figure 6: Simulated diffraction spectra for H/LiF(100) as a function of the azimuthal angle. Left panels: Incidence direction $< 110 >$. Right panels: Incidence direction $< 100 >$. Back (green) solid (dotted) line: The results have been convoluted with a Gaussian function of width σ=0.052 deg. (0.02 deg.) to simulate the experimental resolution of Ref. [9]. E_z (E_T) represents the normal (total) energy, θ_i the polar incidence angle, and z_{av} the classical turning point. Red dashed line: classical reflection probabilities $\times 10$ without bining.

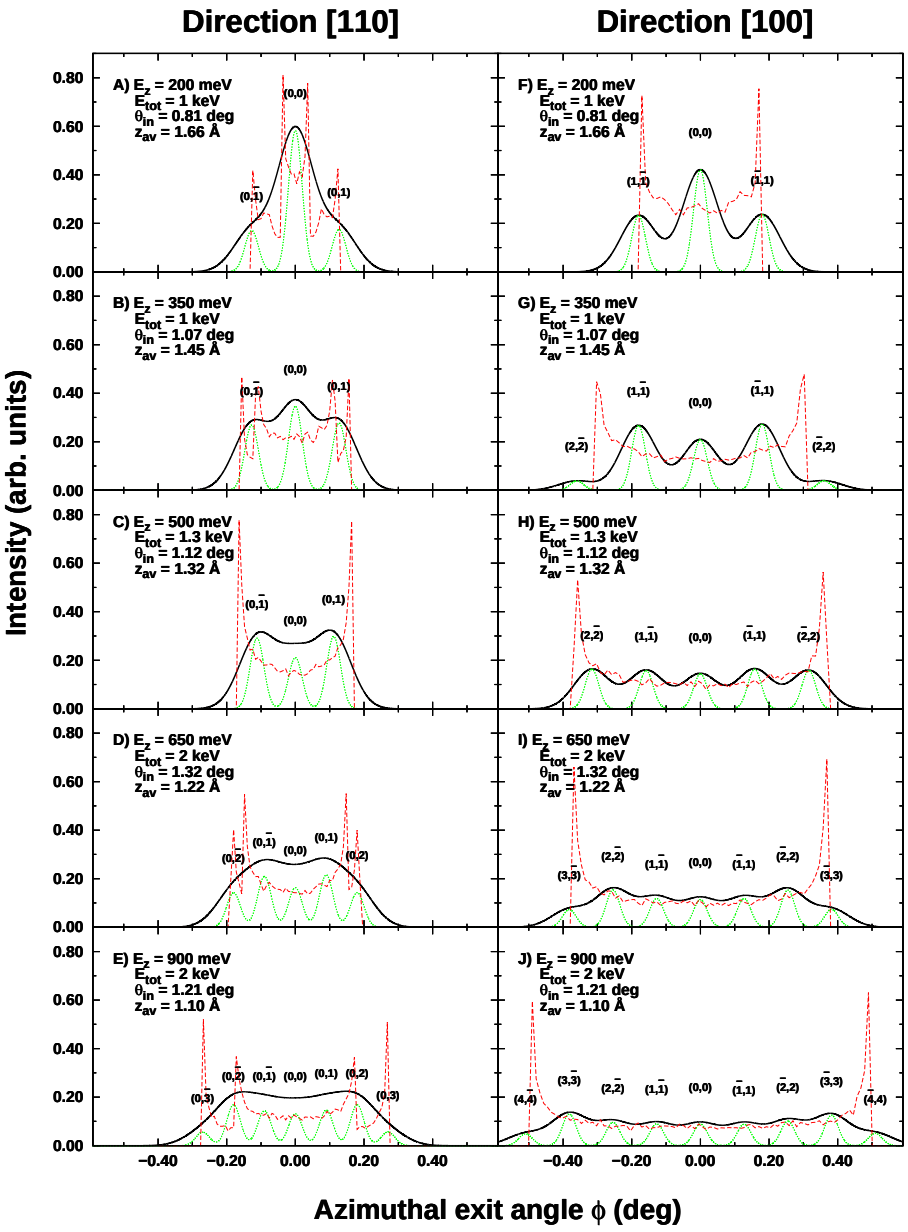

Figure 7: Simulated diffraction spectra for D/LiF(100) as a function of the azimuthal angle. Left panels: Incidence direction $< 110 >$. Right panels: Incidence direction $< 100 >$. Back (green) solid (dotted) line: The results have been convoluted with a Gaussian function of width σ=0.052 deg. (0.02 deg.) to simulate a typical experimental resolution of Ref. [9]. E_z (E_T) represents the normal (total) energy, θ_i the polar incidence angle, and z_{av} the classical turning point. Red dashed line: classical reflection probabilities $\times 10$ without bining.